SCIENCE CHINA
Earth Sciences

Spatio-temporal differentiation of spring phenology in China driven by temperatures and photoperiod from 1979 to 2018

Xiaojing WU, Changxiu CHENG, Cancan QIAO and Changqing SONG

Citation: SCIENCE CHINA Earth Sciences; doi: 10.1007/s11430-019-9577-5

View online: http://engine.scichina.com/doi/10.1007/s11430-019-9577-5

Published by the Science China Press

SCIENCE CHINA
Earth Sciences

•RESEARCH PAPER•

https://doi.org/10.1007/s11430-019-9577-5

Spatio-temporal differentiation of spring phenology in China driven by temperatures and photoperiod from 1979 to 2018

Xiaojing WU[1,2,3,4], Changxiu CHENG[1,2,3,4*], Cancan QIAO[3] & Changqing SONG[1,3,4]

[1] *State Key Laboratory of Earth Surface Processes and Resource Ecology, Beijing Normal University, Beijing 100875, China;*
[2] *Key Laboratory of Environmental Change and Natural Disaster, Beijing Normal University, Beijing 100875, China;*
[3] *Faculty of Geographical Science, Beijing Normal University, Beijing 100875, China;*
[4] *Center for Geodata and Analysis, Beijing Normal University, Beijing 100875, China*

Received September 16, 2019; revised December 17, 2019; accepted January 10, 2020; published online March 24, 2020

Abstract Large amounts of data accumulated in ecology and related environmental sciences arouses urgent need to explore useful patterns and information in it. Here we propose coclustering-based methods and a temperatures-photoperiod driven phenological model to explore spatio-temporal differentiation in long-term spring phenology in China. First, we created the first bloom date (FBD) dataset in China from 1979 to 2018 using the extended spring indices and China Meteorological Forcing Dataset. Then we analyzed the dataset using Bregman block average co-clustering algorithm with I-divergence (BBAC_I) and *k*-means algorithm. Such analysis delineated the spatially-continuous phenoregions in China for the first time. Results showed three spatial patterns of FBD in China and their temporal dynamics for 40 years (1979–2018). More specifically, overall late spring onsets occur in 1979–1996, in which areas located in Jiangxi, northern Xinjiang and middle Inner Mongolia experienced constant changing spring onsets. Overall increasingly earlier spring onsets occur in 1997–2012, in which areas located in Fujian, Hunan and eastern Heilongjiang experienced the most variable spring onsets. Stable early spring onsets over China occur after 2012. Results also showed 15 temporal patterns of spring phenology over the study period and their spatial delineation in China. More specifically, most areas in China have the same FBD category for 40 years while northern Guizhou, Hunan and southern Hubei have the same category in 1979–1997 and then fluctuate between different categories. Finally, our results have certain directive significance on the design of existing observational sites in Chinese Phenological Network.

Keywords First bloom date, Co-clustering, Big data, Spatio-temporal differentiation, Temperatures-photoperiod driven phenological model

Citation: Wu X, Cheng C, Qiao C, Song C. 2020. Spatio-temporal differentiation of spring phenology in China driven by temperatures and photoperiod from 1979 to 2018. Science China Earth Sciences, 63, https://doi.org/10.1007/s11430-019-9577-5

1. Introduction

Unprecedented amounts of data for ecology and related environmental sciences are accumulated due to advances in data collection technologies, such as sensors and modelling (Kelling et al., 2009; Zhu et al., 2017; Cheng et al., 2018; Li et al., 2019). Traditional satellite remote sensing systems and new initiatives in near-surface remote sensing platform can gather data with various spatial and temporal resolutions at any time (La Salle et al., 2016; Guo et al., 2018). Besides, modelling and measurements are also advancing the data accumulation from various sources (Chen et al., 2011). Such big data arouses urgent need to gain insights into important features in it and further reveal patterns and information of potential use (Kelling et al., 2009; Kisilevich et al., 2010).

Spatial and temporal differentiations are important features in the study of ecology and also phenology of ecosystems (Dutilleul, 2011; Wang et al., 2016). Plant phenology studies

* Corresponding author (email: chengcx@bnu.edu.cn)

the life circle phases in plants driven by environmental factors and the study of its long-term patterns and dynamics is significant to understand the terrestrial ecosystems (Zhu and Wan, 1973; Schwartz et al., 2006; Fang and Chen, 2015; Wang et al., 2019). As one of the most reliable bioindicators of climate change, spring events of plant phenology have been proven of inhomogeneity across space and time in many studies (White et al., 2009; Gordo and Sanz, 2010; Jeong et al., 2011; Wu and Liu, 2013). For instance in the Northern Hemisphere, the earlier spring onset in middle and high latitudes are more obvious than that in other regions and they are also more outstanding in the 1980s and 1990s than that in other periods (Piao et al., 2006). These findings make it necessary to study the spatial and temporal differentiations of spring phenology.

There are several methods for collecting materials of spring phenology. The first method relies on site observations of biological events (e.g. first leaf and flower blooming) for selected species. However, the spatial distribution of these phenological observations is poor, even with long-term records (White et al., 2005). The second method is deriving spring onsets using time series of remote sensing satellite images. Nevertheless, the results rely on the adopted method because no methods are universally accepted for characterizing spring onsets from satellite data (White et al., 2009). Moreover, large amounts of satellite data are only collected since the 1980s, which is not sufficient to study the long-term responses of phenology to climate change. The last method uses phenological models, which allow to simulate and predict spring onsets in those regions without observations. Several studies have proved that temperatures and photoperiod are two important driven factors for plant phenology (Schwartz et al., 2006; Gordo and Sanz, 2010; Piao et al., 2015). Thus, in this study we use a temperatures-photoperiod driven phenological model (Section 2.2) to simulate long-term spring onsets (Schwartz et al., 2013).

By partitioning data elements into groups and considering them at an abstract level, clustering is one of the most widely used methods to study the spatio-temporal differentiation of phenology (Andrienko et al., 2009). It is especially useful in the studies of ecology and related environmental science, because the analysis for a given region and a time period generally yields more informative results than that for a few locations and timestamps (Zirlewagen and von Wilpert, 2010). Several studies have applied clustering on the analysis of spatial and temporal differentiations (Ahas and Aasa, 2003; White et al., 2005; Kumar et al., 2011; Zhang et al., 2012). For instance, Ahas and Aasa (2003) applied clustering to analyze temporal differentiation in phenological events by grouping years to early and late years based on seasonal rhythm. Zhang et al. (2012) analyzed spatial differentiation of phenology in the Upper Colorado River Basin by using both principal component analysis and *k*-means++. However, differentiations identified by only using spatial clustering are incapable to illustrate the time-varying behavior in the phenology and vice versa (Deng et al., 2011). Thus, a clustering method that allows to concurrently analyze spatial and temporal differentiations is required to illustrate the spatio-temporal varying behavior in the phenology. By simultaneously performing spatial and temporal clustering, co-clustering methods are able to reveal the variations in phenology both across space and time. Therefore, this study uses co-clustering analysis (Section 2.3) to explore spatio-temporal differentiation of phenology (Wu et al., 2015, 2016).

Based on above, we conduct an exhaustive exploration of spatial and temporal differentiations of spring phenology by using a coclustering-based method: we first use a temperatures-photoperiod driven phenological model and long-term meteorological datasets to create first bloom dates (FBD) dataset; then we perform the co-clustering analysis on the dataset and further visually analyze the co-clustering results to reveal spatio-temporal differentiation of spring phenology.

2. Materials and methods

2.1 Data and computational platform

The China Meteorological Forcing Dataset (http://westdc.westgis.ac.cn/data/7a35329c-c53f-4267-aa07-e0037d913a21; Chen et al., 2011) is used in this study. With the spatial resolution of 0.1°×0.1°, this gridded dataset, covering from 18.2°N to the northern border 53.6°N and from 73.4°E to the eastern border 135°E. With the temporal resolution of 3 hours, this dataset runs from 1979 to 2018. For this study, air temperatures (instantaneous near surface, 2 m) were downloaded and daily maximum (TX) and minimum (TN) temperatures were calculated as the input parameters for the temperatures-photoperiod driven phenological model (Section 2.2).

To assure the completeness of the dataset, we examined TX and TN and excluded grid cells whose FBD could not be calculated for more than 20 years from the phenological model. It resulted into new temperature datasets with 74154 grids for 40 years (1979–2018), whose spatial extent is exemplified in Figure 1 by the spatial distribution of the maximum temperature in one arbitrary day (2018-02-01).

The phenological observational records are used in this study to assess the accuracy of FBD calculated from the phenological model. Here we use those records collected by the Chinese Phenological Network (CPON) and the dataset is supported by National Earth System Science Data Sharing Infrastructure, National Science & Technology Infrastructure of China (http://www.geodata.cn). Administrated by Chinese Academy of Sciences (CAS), CPON includes 44 observational sites (Figure 2) across the country from 1963 to 2008 (Ge et al., 2014, 2015; Wang et al., 2015a, 2015b). Lilac

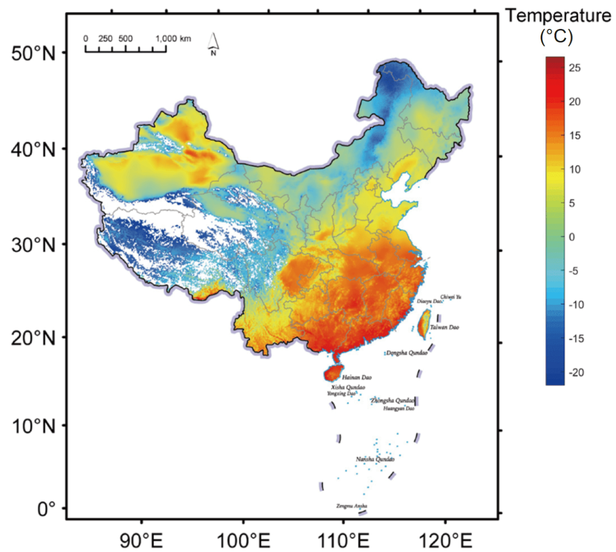

Figure 1 The spatial extent of the meteorological dataset exemplified by the spatial distribution of the maximum temperature in one arbitrary day (2018-02-01).

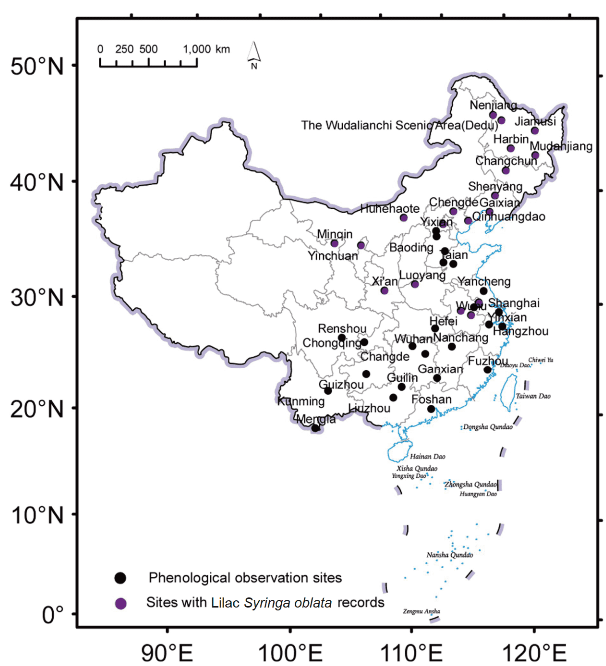

Figure 2 The 44 phenological observational sites in Chinese Phenological Network.

Syringa oblata is selected as the species for the assessment because it is commonly observed in the national network (Schwartz and Chen, 2002). Besides, it was successively used in China for assessing the performance of the spring indices, a previous version of the phenological model we used in this work (Schwartz et al., 2006).

To process the meteorological datasets with high spatio-temporal resolutions and also long time series of FBD, we conducted our experiment on a high-performance computing platform using parallel computing on a blade cluster of three nodes. Each node is configured with two Intel Xeon Gold 6132 CPU (2.60 GHz), 96 GB of Radom Access Memory (RAM) and 240 GB of hard disk space. During the process, deca-core parallel computing was observed within each node.

2.2 Extended spring indices

As a series of regression-based temperatures-photoperiod driven models, the extended spring indices (SIx) are widely used to simulate and predict spring onsets (Schwartz et al., 2013; Izquierdo-Verdiguier et al., 2018). These models remove chilling and warmth requirements from the original spring indices models and thus allow to cover larger areas (Schwartz et al., 2013). Developed using three key species as lilac (*Syringa chinesis*) and honeysuckles (*Lonicera tatarica* and *Lonicera Korolkowii*), SIx mainly predict their first leaf dates (FLD) and FBD.

The inputs for SIx are daily maximum temperature, daily minimum temperature and the latitudinal information for a location, in which the last parameter is used to represent the day length to account for photoperiodic changes (Basler and Körner, 2012). The predicted SIx FBD is the focus of this study for its easiness of observation (Lu, 2006). This index is the average value of the first bloom dates of above three species and represents the onset of late spring. SIx FBD has also been proved to be related to a general onset of vegetative growth in dominant forest vegetation (Schwartz and Chen, 2002). The equation for calculating SIx FBD is as below:

$$\begin{aligned} &\mathrm{FBD}_{ij} = \mathrm{SIx}\left(\mathrm{TX}_{ij}, \mathrm{TN}_{ij}, \mathrm{lat}_{i}\right), \\ &i = 1, \ldots, 74154;\ j = 1, \ldots, 40 \end{aligned} \tag{1}$$

where TX and TN are the daily maximum and minimum temperatures and lat is the latitude. The indices i and j represents the 74154 grid cells of the study area and the 40 years of the study period respectively. TX and TN are of the Fahrenheit unit as required for calibrating SIx. Refer to (Ault et al., 2015) for more detailed description of SIx FBD.

2.3 Co-clustering analysis

Either spatial clustering or temporal clustering is one-way clustering. Take the FBD example dataset in Figure 3a for example. Spatial clustering (Figure 3b) sees the locations of the dataset as objects and timestamps as attributes, which results in location-clusters with similar values along all timestamps, e.g. location-cluster1 (the thick lines in Figure 3b). Temporal clustering sees the timestamps of the dataset as objects and locations as attributes, which results in timestamps with similar values along all locations, e.g. timestamp-cluster1 (the thick lines in Figure 3c). Typically, the clustering method used for spatial clustering is also applic-

(a)

FBD example data	timestamp-1	timestamp-2	timestamp-3	timestamp-4
location-1	101	102	100	55
location-2	100	101	100	55
location-3	102	102	101	160
location-4	60	58	150	70

Spatial clustering

(b)

	FBD example data	timestamp-1	timestamp-2	timestamp-3	timestamp-4
location-cluster1	location-1	101	102	100	55
	location-2	100	101	100	55
	location-3	102	102	101	160
	location-4	60	58	150	70

Temporal clustering

Spatio-temporal co-clustering

(c)

	timestamp-cluster1			
FBD example data	timestamp-1	timestamp-2	timestamp-3	timestamp-4
location-1	101	102	100	55
location-2	100	101	100	55
location-3	102	102	101	160
location-4	60	58	150	70

(d)

		timestamp-cluster1			
	FBD example data	timestamp-1	timestamp-2	timestamp-3	timestamp-4
location-cluster1	location-1	101	102	100	55
	location-2	100	101	100	55
	location-3	102	102	101	160
	location-4	60	58	150	70

Figure 3 One-way and co-clustering analysis of FBD example dataset. (a) An FBD example dataset; (b) spatial clustering resulting in location-clusters with similar values along all timestamps, e.g. location-cluster1 (the thick line); (c) temporal clustering resulting in timestamp-clusters with similar values along all locations, e.g. timestamp-cluster1 (the thick line); (d) spatio-temporal clustering resulting in spatio-temporal co-clusters with similar values along both locations and timestamps, e.g. the intersection of location-cluster1 and timestamp-cluster1 (the thick lines).

able for temporal clustering, e.g. *k*-means.

Being different from one-way clustering, co-clustering sees locations and timestamps the same by grouping locations and timestamps to location-clusters and timestamp-clusters simultaneously (Figure 3d) (Dhillon et al., 2003; Han et al., 2012; Shen et al., 2018). It results in spatio-temporal co-clusters, i.e. the intersection formed by each location- and timestamp- cluster, within each of which values are similar along both locations and timestamps, e.g. the intersection of location-cluster1 and timestamp-cluster1 (the thick lines in Figure 3d).

There have been many studies in various fields that use co-clustering methods for pattern analysis (Dhillon et al., 2003; Banerjee et al., 2007; Wu et al., 2015, 2016). Dhillon et al. (2003) used a co-clustering algorithm named the Information Theoretic Co-clustering (ITCC) for word-document analysis, which adopts the I-divergence metric as distance measure to build the objective function and optimize co-clusters. Banerjee et al. (2007) proposed Bregman co-clustering algorithm with several distance measures including I-divergence and Euclidean distance etc. for optimizing co-clusters. In their applications, the superiority of the I-divergence metric was empirically improved for word-document analysis. Recently, Wu et al. (2015) and Wu et al. (2016) both used the Bregman block average co-clustering algorithm with I-divergence (BBAC_I) to analyze spatio-temporal datasets. As a special case of the Bregman co-clustering algorithm, BBAC_I effectively identified location-timestamp co-clusters and revealed spatial and temporal patterns as well as their dynamics. This algorithm is thus used in this study to analyze spatio-temporal pattern in FBD and further reveal spatial and temporal differentiations of spring phenology.

BBAC_I is typically used to analyze data matrices representing co-occurrences or joint probability between two random variables, which contain positive and real-valued elements (Wu et al., 2015). This algorithm takes the co-clustering issue as an optimization problem in the field of information theory and the optimal co-clustering results minimizes the loss in mutual information between the two matrices before and after the co-clustering analysis. The SIx FBD is organized into a co-occurrence matrix (O_{FBD}) between a spatial and a temporal variables that takes values in 74154 grid cells and 40 years respectively. That is, O_{FBD} is a matrix with its size as 74154×40. The process of optimizing FBD data matrix to the optimal co-clusters by BBAC_I is summarized into three steps as below (Figure 4).

(i) Random initialization. This is to randomly group 74154 grids and 40 years in FBD data matrix O_{FBD} to gc (number of grid-clusters) grid-clusters and yc (number of grid-clusters) year-clusters, which results in the co-clustered FBD data matrix $\widehat{O}_{\mathrm{FBD}}$ with its size as $gc \times yc$.

(ii) Calculating the loss in mutual information. This is to build the objective function using I-divergence to measure the loss in mutual information between O_{FBD} and $\widehat{O}_{\mathrm{FBD}}$:

$$f_{\mathrm{loss}} = D_{\mathrm{I}}\left(O_{\mathrm{FBD}} \,\|\, \widehat{O}_{\mathrm{FBD}}\right), \tag{2}$$

where $D_{\mathrm{I}}(\cdot \,\|\, \cdot)$ means the I-divergence between matrices, which can be used to calculate the loss of mutual information between two matrices.

(iii) Iterations for optimizing the objective function. This is to begin an iterative process to minimize the loss of mutual information by updating the memberships of grid-clusters and year-clusters. This step includes two sub-steps:

(1) The update of membership of grid-clusters. This is to find the grouping from grids to grid-clusters that minimizes

Bregman block average co-clustering algorithm with I-divergence (BBAC_I)

Input: O_{FBD}, gc (number of grid-clusters), yc (number of year-clusters)

Output: optimized co-clusters

Begin

1. Initialization: randomly mapping 74154 grids to gc grid-clusters and 40 years to yc year-cluster;
2. Calculation of the loss function

$$f_{\mathrm{loss}} = D_{\mathrm{I}}(O_{\mathrm{FBD}} \,\|\, \hat{O}_{\mathrm{FBD}})$$

3. Iterations:

3.1 update mapping from grids to grid-clusters

$$i = \arg\min_{i\in\{1,\dots,gc\}} D_{\mathrm{I}}(O_{\mathrm{FBD}} \,\|\, \hat{O}_{\mathrm{FBD}})$$

3.2 update mapping from years to year-clusters

$$j = \arg\min_{i\in\{1,\dots,yc\}} D_{\mathrm{I}}(O_{\mathrm{FBD}} \,\|\, \hat{O}_{\mathrm{FBD}})$$

End

Figure 4 Bregman block average co-clustering algorithm with I-divergence (BBAC_I).

the loss of mutual information according to the objective function:

$$i = \arg\min_{i\in\{1,\dots,gc\}} D_{\mathrm{I}}\left(O_{\mathrm{FBD}} \,\|\, \widehat{O}_{\mathrm{FBD}}\right). \tag{3}$$

(2) The update of membership of year-clusters. This is to find the grouping from years to year-clusters that minimizes the loss of mutual information according to the objective function:

$$j = \arg\min_{i\in\{1,\dots,yc\}} D_{\mathrm{I}}\left(O_{\mathrm{FBD}} \,\|\, \widehat{O}_{\mathrm{FBD}}\right). \tag{4}$$

Studies have proved that the loss of mutual information decreases after each iteration (Banerjee et al., 2007). Then the iterative process ceases when the loss function reaches the convergence of a local minimum (change in the loss is less than a preset threshold). Moreover, because we cannot assure the global optimum, the aforementioned co-clustering process is usually repeated for several times to find the optimal co-clusters to the largest extent. Refer to (Wu et al., 2015) for detailed optimization process of BBAC_I.

Since the co-clustering process assigns full rows and columns to clusters, the co-clustered matrices show a checkboard format with similar neighboring co-clusters (Wu et al., 2016). To better capture the spatio-temporal differentiation in the FBD dataset, we first predefined a large number of co-clusters for BBAC_I, then used *k*-means algorithm to refine these co-clusters into *k* irregular co-clusters which are axis-parallel and non-rectangular. The input for *k*-means is the average FBD value of each co-cluster and the number of *k* was decided using the Silhouette method (Rousseeuw, 1987). Besides, because both BBAC_I and *k*-means are local optimization algorithms, running for multiple times is necessary for optimal and stable co-clustering results. Finally, we used *q* value of Geodetector to evaluate the co-clustering results (Wang and Xu, 2017).

2.4 Spatio-temporal differentiation of spring phenology

To reveal spatio-temporal differentiation in the FBD dataset, small multiples[1)], linear timeline[2)] and geographical map are used to visually analyze the irregular co-clusters. First, we extracted several spatial patterns from the co-clustering results by combining phenoregions, i.e. similar clusters in respect of FBD in this study, in the same year-clusters. Each map in the small multiples was used to visualize the unique spatial patterns over the study area. A linear timeline was used to visualize the temporal dynamics of these spatial patterns over the study period. Then, we extracted several temporal patterns from the co-clustering results by combining years with similar FBD dynamics and arranged them in the chronological order. Each of the set of linear timelines was used to visualize the unique temporal patterns in the study period. A geographical map was used to visualize the grids with the same temporal patterns, that is, the spatial delineation of the study area with similar FBD temporal patterns.

3. Results

3.1 First bloom dates

SIx yielded the FBD values for 74154 grid cells in China from 1979 to 2018 (40 years) using the filtered meteorological datasets. The spatial extent of the dataset is exemplified in Figure 5 using FBD in 2018. The purpler color means the earlier FBD. The figure shows the trend that the FBD are becoming late from south to north of China. It also shows that FBD occur in early spring dates (early March) in southern provinces, such as Yunnan, Guangxi, southern Sichuan etc. while provinces in middle regions, e.g. Shandong and Henan, FBD occur around April. Late FDB (late May) occur in the three provinces in the northeast of China (Heilong, Jilin, Liaoning) while very late FDB (June and afterwards) occur mostly in the Tibet Plateau. It is worth pointing out that even though the spatial trends of FBD (Figure 5) are similar with those of maximum temperatures (Figure 1), they are essentially different. It is because Figure 5 shows the spatial trends of spring phenology of one year whereas Figure 1 shows the trends of one day in that particular year. More importantly, SIx seizes the non-linear property of

1) Small multiples is a visualization that puts a series of geographical maps next to each other, which is mainly used to understand changing features of multivariate information.

2) Linear timeline is one type of timeline, which uses a linear line to visualize events that occur in the order of linear time (e.g. year).

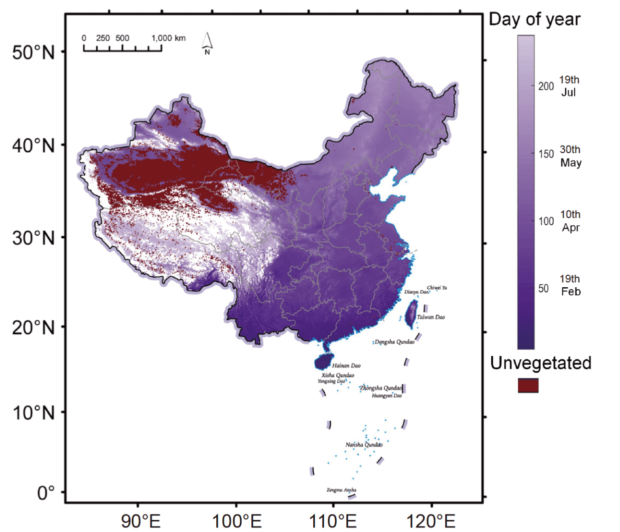

Figure 5 The spatial extent of SIx first bloom dates, exemplified using the year 2018.

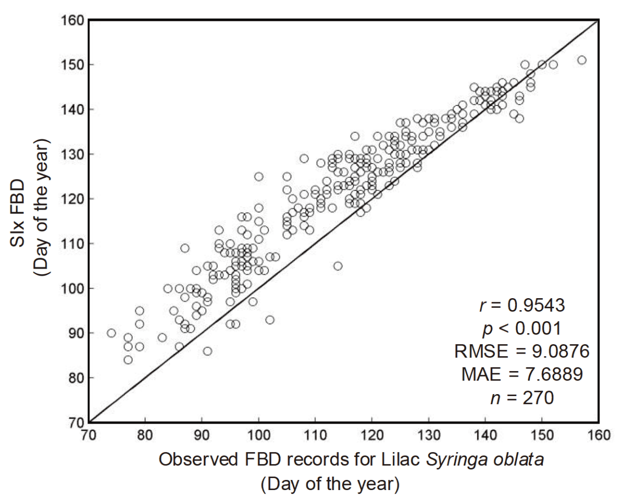

Figure 6 Validation of SIx FDB using the observed FBD records for Lilac *Syringa oblata* from CPON.

temperatures accumulation (Schwartz et al., 2013).

The accuracy of SIx FBD was assessed using the observed records of FBD for Lilac *Syringa oblata* from CPON. According to the observation criteria of CPON (Wan and Liu, 1979), FBD is defined as the date when petals of one or more than three flowers begin their full bloom for more than half of the plants in the selected species. We found 270 observed FBD records for Lilac *Syringa oblata* and extracted the SIx FBD using geographical coordinates and years for these records. Then we used the scatter plots of the SIx and observed records to validate the performance of the models (Figure 6). It shows that SIx FBD and observed FBD are strongly correlated (r=0.9543 and p<0.01).

3.2 Co-clustering results: FBD categories

Based on above, the FBD dataset was organized into a matrix where rows are 74154 grids and columns are 40 years (1979–2018), which was subjected to BBAC_I and k-means algorithms. The number of grid-clusters and year-clusters for BBAC_I were chosen as 495 and three after testing values from 300 to 700 with an interval of 50 and from three to seven respectively. That is because the objective function of the co-clustering algorithm reaches its minimum with these two numbers for the FBD dataset. The numbers of threshold, random mappings and iterations for BBAC_I were empirically set as 200, 3000 and 10^{-6} to guarantee convergence of the objective function as well as the stable results. The number of irregular co-clusters for k-means was set to five using the Silhouette method. Finally, the q value of Geodetector for evaluating the clustering results is 0.9141, indicating good heterogeneity of the co-clustering results (Dong et al., 2017).

The co-clustering analysis resulted in five irregular co-clusters within the FBD dataset. To characterize the whole dataset, we defined the five co-clusters as “very early”, “early”, “intermediate”, “late”, and “very late” FBD categories according to their values. These values (rounded) correspond to late February (58th DOY), early April (102nd DOY), early May (124th DOY), late May (148th DOY) and afterwards (199th DOY), respectively. These five FBD categories are displayed in the heatmap in Figure 7. X-axis is the 40 years of the FBD dataset arranged according to the order of the year-clusters with increasing average values from right to left. The values of y-axis are 74154 grids covered by the dataset arranged according to the grid-clusters with increasing average values from bottom to top. Because BBAC_I orders the matrix based on the average value of a complete row (grid) or column (year), it might occur that different FBD categories are embedded. For instance, the average value of one grid is higher than that of another along all 40 years but lower in subsets of years. Figure 8 shows the spatial distribution of FBD categories, or phenoregions. Each category contains 3 phenoregions because of different spatial extents in different year-clusters.

Figure 7 shows that among all categories, “intermediate” FBD account for the largest proportion, followed by “early” FBD whereas “very late” FBD account for the smallest, then followed by “very early” FBD. It also shows that the years with the largest area of grids for “very early” FBD are mostly recent years. The years with the smallest area of grids for “very early” FBD and largest area of grids for “very late” FBD are the ones before the year 2000, which belong to the first half of the study period. Together with Figure 8, it can be seen that “very early” FBD mostly occur in provinces in the southern regions of China, e.g. Hainan, Guangdong and also southern Sichuan. Besides, this FBD category covers more regions to the north from early years of the study period to recent years. “Early” FBD mostly occur in provinces in middle eastern regions, e.g. Jiangsu and Anhui. “Inter-

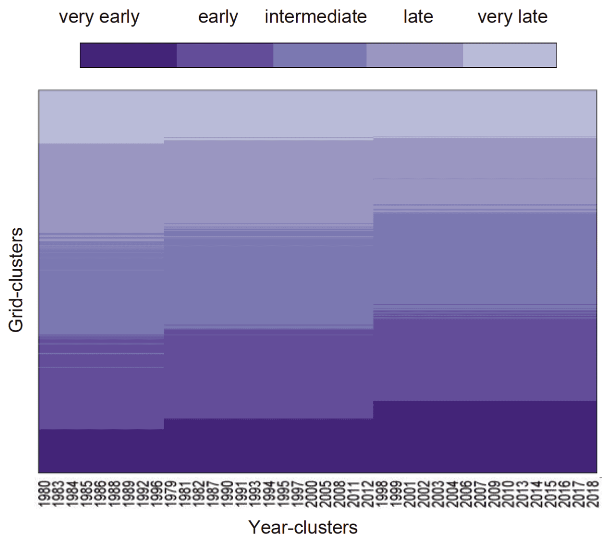

Figure 7 The co-clustering results defined as "very early", "early", "intermediate", "late", and "very late" FBD categories to characterize the whole dataset. *X*-axis is 40 years of the FBD dataset arranged according to the order of the year-clusters with increasing average values from right to left. *Y*-axis is 74154 grids covered by the dataset arranged according to grid-clusters with increasing average values from bottom to top.

mediate" FBD occur in provinces in middle and northern regions, e.g. Ningxia and three northeast provinces. "Late" FBD occur in provinces in northern China while "very late" FBD occur mostly in Tibetan Plateau.

3.3 Spatio-temporal differentiation of FBD

These five FBD categories in the FBD dataset were further visually analyzed to display the multiple spatial patterns and their temporal dynamics as well as multiple temporal patterns and their spatial distribution, and thus reveal spatio-temporal differentiation of spring phenology.

3.3.1 Spatial patterns and their temporal dynamics

Three spatial patterns over the whole study area are composed by combining grids that have the same variation throughout China in Figure 7, i.e. phenoregions in the same year-cluster. They are named Spatial patterns1–3. The small multiples in the left of Figure 9 shows these three spatial patterns and the linear timeline in the right of Figure 9 shows their temporal dynamics from 1979 to 2018. Table 1 shows the percentages of FBD categories for each spatial pattern and the number of years that exhibit each pattern.

In Spatial pattern3, "very early" FBD account for the highest percentages and "late" and "very late" FBD for the lowest while in Spatial pattern1, "very early" FBD account for the lowest percentages and "late" and "very late" FBD for the highest. Then changes from Spatial pattern1 to Spatial pattern3 give rise to 7.35% increases in phenoregions of "very early" FBD, mainly located in provinces of Guizhou, Hunan, Jiangxi, Fujian and also eastern regions of Sichuan. Such changes also result in 6.41% and 1.56% decreases in phenoregions of "late" and "very late" FBD, which are mainly located in northern Xinjiang, northeastern Inner Mongolia and southern Heilongjiang. Thus, changes from Spatial pattern1 to Spatial pattern3 indicate increasingly early FBD and spring onsets. Besides, changes from Spatial pattern1 to Spatial pattern2 also result in increases in phenoregions of "very early" FBD (2.76%) and decreases in phenoregions of "late" (1.9%) and "very late" (1.09%) FBD, which indicate increasingly early FBD and spring onsets. These areas are mainly distributed in Jiangxi province for the former and northern Xinjiang, middle area of Inner Mongolia for the latter. On the contrary, variations from Spatial pattern3 to Spatial pattern2 result in decreases in phenoregions of "very early" FBD (4.59%), mainly located in Hunan and Fujian. The variations also result in the increases in phenoregions of "late" FBD (4.51%), mainly distributed in eastern Heilongjiang. Such variations mean increasingly late FBD and spring onsets.

The temporal dynamics of these three spatial patterns in the timeline shows a general increasingly earlier trend of FBD from early to recent years. Almost half of years in the study period (16 out of 40) exhibit Spatial pattern3 and focus on the recent years after 1997 while less than one fourth (9 out of 40) years exhibit Spatial pattern1 and focus on the early period before 1997. As such, three time periods appear for different variations of FBD over the study period: 1979–1996, 1997–2012 and 2012–2018. In the period of 1979–1996, variations are among Spatial pattern1 and Spatial pattern2, indicating overall late spring onsets. Areas located in Jiangxi, northern Xinjiang and middle Inner Mongolia experienced constant changing spring onsets in this period. In the period of 1997–2012, variations are among Spatial pattern2 and Spatial pattern3, indicating overall increasingly earlier spring onset. Areas located in Fujian, Hunan and eastern Heilongjiang have the most variable spring onsets in this period. Years after 2012 focus on Spatial pattern3, indicating stable early spring onsets over China. Besides, the biggest variation of FBD occurred from 1996 to 1998, in which areas located in Guizhou, Hunan, Jiangxi, Fujian, eastern regions of Sichuan, northern Xinjiang, middle Inner Mongolia and southern Heilongjiang experienced increasingly earlier spring onset.

3.3.2 Temporal patterns and their spatial distribution

The timelines in Figure 10a displays the 15 temporal patterns over the study period that are composed by combining years that have the same variation in Figure 7. These temporal patterns can be divided into five categories according to the changing state of FBD: stable (1st row), first stable and then fluctuant (2nd row), first fluctuant and then stable (3rd row), frequently fluctuant (1st column of the 4th row) and drastic fluctuant (2nd column of the 4th row). The spatial distribu-

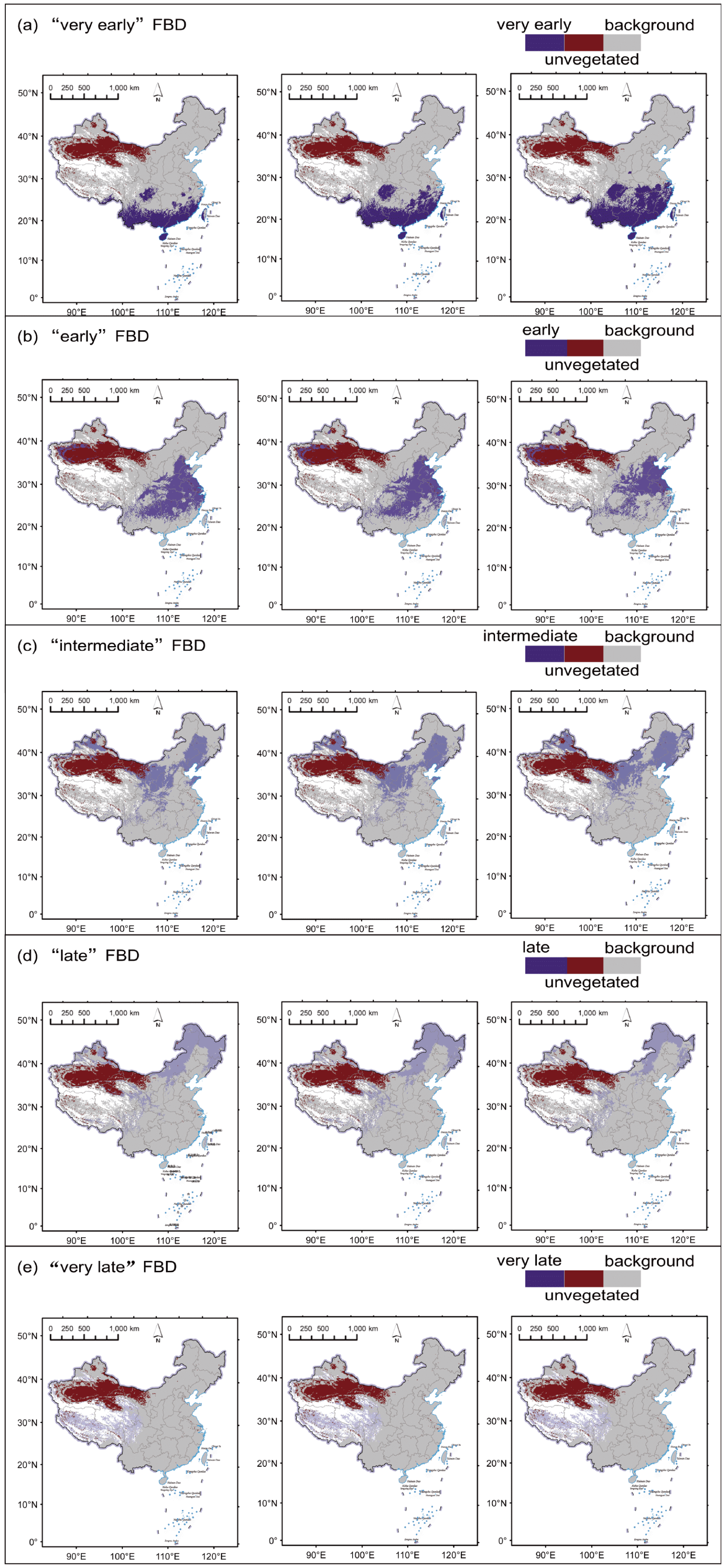

Figure 8 Phenoregions for each of the five FBD categories.

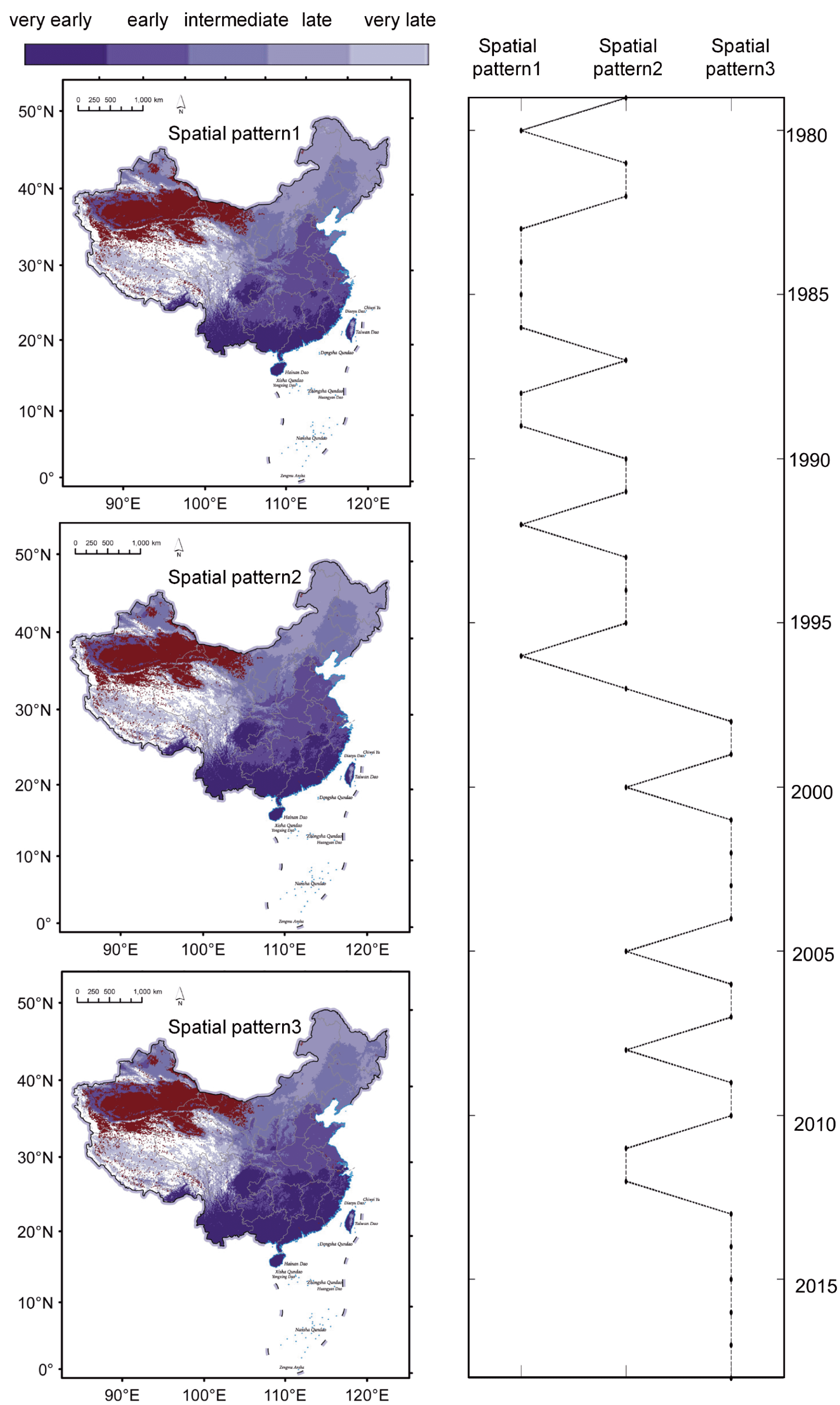

Figure 9 Three spatial patterns and their temporal dynamics in the FBD dataset.

tion of each temporal pattern is displayed in the geographical map in Figure 10b with different categories using different colors. Table 2 shows the percentages of each category as well as the temporal patterns in the map.

Among the five FBD changing states, the stable state accounts for the highest percentage (more than 75%) and has the widest spatial distributions, followed by first stable and then fluctuant state while drastic fluctuant state accounts for the lowest (less than 0.02%). The stable state of FBD is barely influenced by climate change, in which the temporal pattern of "late" FBD lasting for 40 years takes the largest percentage (18.58%), mainly distributed in eastern Inner Mongolia and Heilongjiang. The temporal patterns of "intermediate" FBD lasting for 40 years takes the second largest percentage, mainly distributed in Liaoning and middle western Jilin. It is followed by the temporal patterns of

Table 1 Percentages of FBD categories per spatial pattern and the number of years taken by each spatial pattern

Spatial patterns	“very early” FBD	“early” FBD	“intermediate” FBD	“late” FBD	“very late” FBD	Number of years
Spatial pattern1	11.42%	23.65%	25.62%	25.41%	13.90%	9
Spatial pattern2	14.18%	23.57%	25.93%	23.51%	12.81%	15
Spatial pattern3	18.77%	23.22%	26.67%	19.00%	12.34%	16

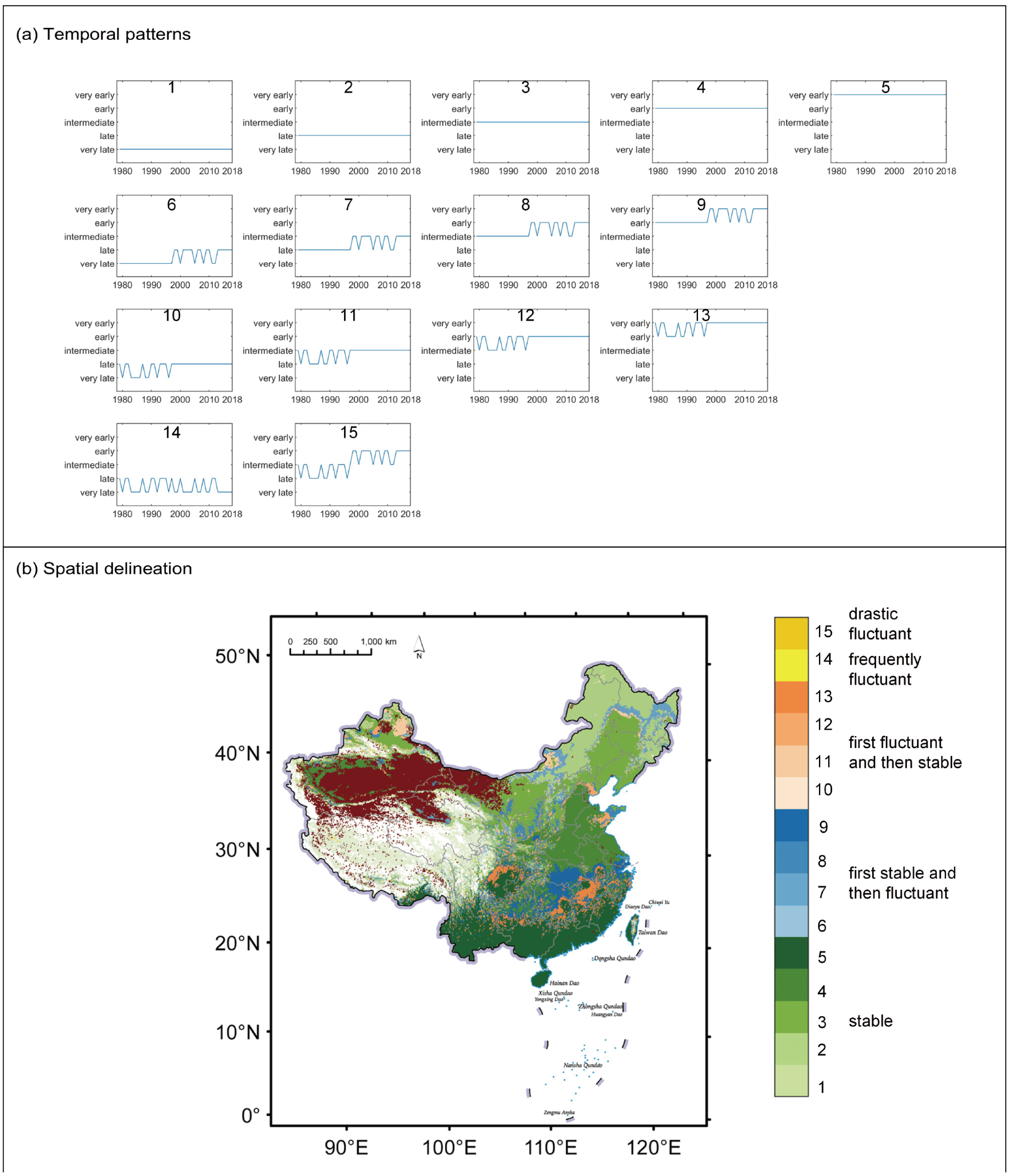

Figure 10 Fifteen temporal patterns in the FBD dataset and their spatial delineation.

“early” and “very early” FBD lasting for 40 years, with the former distributed in southern Hebei, western Shandong, Henan, Anhui and Jiangsu and the latter distributed in southern Yunnan, Guangxi, Guangdong and southern Fujian. The temporal pattern of “very late” FBD lasting for 40 years takes the smallest percentage distributed in Tibetan Plateau, western Sichuan and eastern Qinghai.

The states of first stable and then fluctuant and first fluctuant and then stable are less impacted by climate change. In the state of first stable and then fluctuant, the temporal pattern of “early” FBD in 1979–1997 and then fluctuating between “early” and “very early” FBD takes the largest

Table 2 Percentages of each category and the temporal patterns in the map

FBD change states	Temporal patterns	Percentage	Sum of percentage
Stable	"very late" for 40 years	12.67%	75.06%
	"late" for 40 years	18.58%	
	"intermediate" for 40 years	17.14%	
	"early" for 40 years	13.49%	
	"very early" for 40 years	13.18%	
First stable and then fluctuant	stable: "very late" fluctuant: "very late" & "late"	0.72%	14.17%
	stable: "late" fluctuant: "late" & "intermediate"	4.94%	
	stable: "intermediate" fluctuant: "intermediate" & "early"	3.23%	
	stable: "early" fluctuant: "early" & "very early"	5.28%	
First fluctuant and then stable	fluctuant: "very late" & "late" stable: "late"	0.88%	9.19%
	fluctuant: "late" & "intermediate" stable: "intermediate"	2.96%	
	fluctuant: "intermediate" & "early" stable: "early"	2.17%	
	fluctuant: "early" & "very early" stable: "very early"	3.18%	
Frequently fluctuant	"late" & "very late"	0.23%	0.23%
Drastic fluctuant	"late" & "intermediate" & "early"	0.0186%	0.0186%

percentage (5.28%), mainly distributed in northern Guizhou, Hunan and southern Hubei. It is followed by the temporal pattern of "late" FBD in 1979–1997 and then fluctuating between "late" and "intermediate" FBD, which is mainly distributed in southern Heilongjiang and middle areas of Inner Mongolia. In the state of first fluctuant and then stable, the temporal pattern of fluctuating between "early" and "very early" FBD in 1979–1997 and then stable for "very early" FBD accounts for the highest percentage (3.18%), mainly distributed in some areas in eastern Sichuan, southeastern Hunan and northern Jiangxi.

The states of frequently fluctuant and drastic fluctuant are heavily influenced by climate change but they take very small percentages with very narrow spatial distribution. The former frequently fluctuates between "very late" and "late" FBD for 40 years, mainly distributed in few grids in eastern and western Tibet, middle Xinjiang and northeastern Inner Mongolia. The latter frequently fluctuates between "late" and "intermediate" FBD in 1979–1997 and between "intermediate" and "early" FBD in 1998–2018, mainly distributed in very few grids in northeastern Tibet and eastern Taiwan.

4. Discussion

Many studies have explored spatial and temporal differentiations of spring phenology in China using satellite-based land surface phenology and also ground phenological observations. For instance, Ge et al. (2015) conducted a meta-analysis of phenology in China using the phenological time series across 145 sites from 1960 to 2011. They found that most of records shift toward earlier spring onset. Such trends can be also observed in Figure 9 in our study. Using AVHRR NDVI dataset in temperate China from 1982 to 2010, Cong et al. (2013) found widespread earlier spring onsets in Inner Mongolia using Polyfit. Our results confirmed those findings by observing increasingly early spring onsets in the middle area of Inner Mongolia when temporal dynamics changes from Spatial pattern1 to Spatial pattern2 from 1979 to 1996 (Figure 9). Wang et al. (2015b) analyzed spatial patterns of spring phenological records observed across 22 stations in China from 1963 to 2012 and found that southwestern China exhibit the maximum variability. Results in our study confirmed these findings: as showed in Figure 9, the variations among spatial patterns in the period of 1979–1996 and 1997–2012 result in variabilities of early/late spring onsets in southwestern China, such as Guizhou, Hunan, Jiangxi and Sichuan. Besides, many studies have found the changing point of spring phenology in the middle or late 1990s. For instance, using NOAA/AVHRR NDVI dataset in China from 1982 to 2012, Peng et al. (2011) analyzed spatio-temporal differentiation in spring phenology and found out that there is outstanding earlier trend of spring onset from 1982 to 1998 while such trend becomes weakened from 1998 to 2012. The changing point is almost the same with the one found in our results (the year 1997), which might because that we used FBD in this study. Using AVHRR NDVI dataset in China from 1982 to 2012, Ge et al. (2016) analyzed spring phenological patterns and found later spring onsets from 1982 to 1995 and earlier spring onsets from 1996 to 2008. Although with the turning point one year later at 1997 that might due to the extent of the study period (1979–2018 in our study), our results show similar temporal dynamics of spring onsets: overall late spring onsets from 1979 to 1996 and earlier spring onsets from 1996 to 2008. Above results all show the capability of co-clustering and SIx for exploring spatial patterns and their temporal dynamics as well as temporal patterns and their spatial distributions of spring phenology and further revealing the spatio-temporal differentiation.

Compared with those studies cited above, our study simulates long-term spring onsets for large regions by using SIx. By this means, we delineated the first spatially contiguous phenoregions over China while several phenological regionalizations already exist in Europe and CONUS (Zhang et al., 2012, Wu et al., 2016). These spatially-continuous phenoregions provide more detailed information than the analysis using weather stations and ground observations that are not evenly distributed (Kumar et al., 2011; Wu et al., 2016). Moreover, by applying co-clustering method for analyzing spring phenology in China, our results discover multiple spatial patterns as well as their temporal dynamics. By further visual analysis, the coclustering-based analysis enable the simultaneous identification of locations with the most variable spring onsets for certain time periods and of the time period when the biggest variation occurs in specific locations. Our results also discover several temporal patterns and their spatial distribution in the study area.

Besides, results in this study can also be used to assess and provide suggestions on the design of existing sites in CPON. There have been studies on assessing the design of observational sites of ecological monitoring network in other countries, e.g. in USA (Hoffman et al., 2013). By overlapping the 44 observational sites in CPON with the spatial delineation map of temporal patterns in FBD, the distribution of existing sites in different changing states of FBD can be seen (Figure 11). Almost 60% of existing sites (26 out of 44 sites) belong to the stable state, e.g. sites in Nenjiang of Heilongjiang, Shenyang of Liaoning, Dezhou of Shandong and Foshan of Guangdong, etc. All other sites belong to the state of first stable and then fluctuant, e.g. sites in Jiamusi of Heilongjiang, Wuhan of Hubei and Changde of Hunan, or the state of first fluctuant and then stable, e.g. sites in Renshou of Sichuan and Nanchang of Jiangxi. Few sites exist in the western region of China. Thus, based on different characteristics of the changing states in FBD, this study suggests that more observational sites of FBD should be added in the areas that belong to the states of first stable and then fluctuant

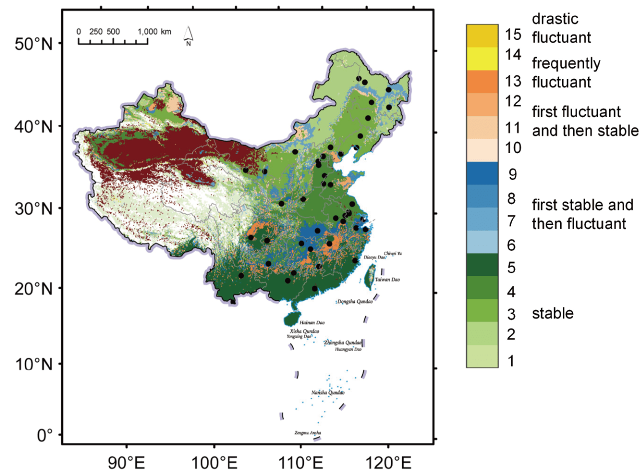

Figure 11 The spatial delineation of FBD dataset and existing observational sites in CPON.

and also of first fluctuant and then stable, e.g. Jiangxi, Hunan, Hubei, Chongqing, northeastern Sichuan and southern Heilongjiang. Moreover, observational sites should be added in western areas in China, e.g. northern Xinjiang and Qinghai and the addition of these sites should also consider their distances from cities (Chu et al., 2017). Besides, the management of agriculture and forestry should be strengthened in the fluctuant areas as aforementioned (Ruml and Vulić, 2005).

Finally, regarding the driving factors of multiples spatial and temporal patterns of spring phenology in the results, we think that they are mainly influenced by daily maximum and minimum temperatures as well as photoperiods. Because this study used SIx to simulate FBD and its input parameters are daily maximum/minimum temperatures and latitude that represent day length to indicate the change of photoperiod (Schwartz et al., 2013). However, in the future studies we will consider the impacts of other factors on spatio-temporal patterns of spring phenology, e.g. climatic zones, altitudinal zones, monsoon belt, precipitation as well as their interactions (Fang and Chen, 2015).

5. Conclusion

In this study, we have used the coclustering-based method and a temperatures-photoperiod driven phenological model to explore spatio-temporal differentiation of long-term spring phenology in China. First, we created and validated the FBD dataset in China from 1979 to 2018 using SIx and China Meteorological Forcing Dataset. Then we used both BBAC_I and *k*-means algorithms to analyze the FBD dataset, which resulted in irregular co-clusters with similar FBD along both spatial and temporal dimensions. Finally, spatio-temporal differentiation in spring phenology were visually explored from these co-clusters.

The coclustering-based analysis in our study delineated the spatially-continuous phenoregions in China for the first time. Such analysis resulted in three spatial patterns of FBD in China and their temporal dynamics for 40 years (1979–2018). More specifically, different variations of FBD appear for three time periods: 1979–1996, 1997–2012 and 2012–2018. Overall late spring onsets occur in 1979–1996 and areas located in Jiangxi, northern Xinjiang and middle Inner Mongolia experienced constant changing spring onsets in this period. Overall increasingly earlier spring onset occur in 1997–2012 and areas located in Fujian, Hunan and eastern Heilongjiang have the most variable spring onsets in this period. Stable early spring onsets over China occur after the year 2012. Besides, the biggest variation of FBD occurred in 1996–1998 and areas located in southwestern and northeastern China experienced increasingly earlier spring onsets. The analysis also resulted in 15 temporal patterns of spring phenology over the study period and their spatial delineation in China. More specifically, most areas in China belong to the stable state, i.e. the same FBD category for 40 years while northern Guizhou, Hunan, southern Hubei, southern Heilongjiang and middle areas of Inner Mongolia belong to the state of first stable in 1979–1997 and then fluctuant.

Acknowledgements *We thank the high-performance computing support from the Center for Geodata and Analysis, Faculty of Geographical Science, Beijing Normal University (https://gda.bnu.edu.cn/). Besides, the forcing dataset used in this study was developed by Data Assimilation and Modeling Center for Tibetan Multi-spheres, Institute of Tibetan Plateau Research, Chinese Academy of Sciences. The phenological data is supported from "National Earth System Science Data Sharing Infrastructure, National Science & Technology Infrastructure of China. (http://www.geodata.cn)". We also thank Prof. Dr. Raul Zurita-Milla for assistance with SIx models and Prof. Wenquan Zhu and Prof. Yongmei Huang for constructive comments. This research was supported by the National Key R&D Program of China (Grant No. 2019YFA0606901), the National Natural Science Foundation of China (Grant No. 41901317) and the China Postdoctoral Science Foundation (Grant No. 2018M641246).*

References

Ahas R, Aasa A. 2003. Developing comparative phenological calendars. In: Schwartz M D, ed. Phenology: An Integrative Environmental Science. Springer Netherlands. 301–318

Andrienko G, Andrienko N, Rinzivillo S, Nanni M, Pedreschi D, Giannotti F. 2009. Interactive visual clustering of large collections of trajectories. Atlantic City: IEEE Symposium on Visual Analytics Science and Technology (VAST)

Ault T R, Zurita-Milla R, Schwartz M D. 2015. A Matlab© toolbox for calculating spring indices from daily meteorological data. Comput Geosci, 83: 46–53

Banerjee A, Dhillon I, Ghosh J, Merugu S, Modha D S. 2007. A generalized maximum entropy approach to bregman co-clustering and matrix approximation. J Mach Learn Res, 8: 1919–1986

Basler D, Körner C. 2012. Photoperiod sensitivity of bud burst in 14 temperate forest tree species. Agric For Meteorol, 165: 73–81

Chen Y Y, Yang K, He J, Qin J, Shi J C, Du J Y, He Q. 2011. Improving land surface temperature modeling for dry land of China. J Geophys Res, 116: D20104

Cheng C X, Shi P J, Song C Q, Gao J P. 2018. Geographic big-data: A new opportunity for geography complexity study (in Chinese). Acta Geogr Sin, 73: 5–14

Chu H, Baldocchi D D, John R, Wolf S, Reichstein M. 2017. Fluxes all of the time? A primer on the temporal representativeness of FLUXNET. J Geophys Res-Biogeosci, 122: 289–307

Cong N, Wang T, Nan H J, Ma Y C, Wang X H, Myneni R B, Piao S L. 2013. Changes in satellite-derived spring vegetation green-up date and its linkage to climate in China from 1982 to 2010: A multimethod analysis. Glob Change Biol, 19: 881–891

Deng M, Liu Q L, Wang J Q, Shi Y. 2011. A general method of spatio-temporal clustering analysis. Sci China Inf Sci, 56: 1–14

Dhillon I S, Mallela S, Modha D S. 2003. Information-theoretic co-clustering. Washington D C: The 9th International Conference on Knowledge Discovery and Data Mining (KDD). 89–98

Dong Y X, Xu Q, Yang R, Xu C D, Wang Y Y. 2017. Delineation of the northern border of the tropical zone of China's mainland using Geodetector (in Chinese). Acta Geogr Sin, 72: 135–147

Dutilleul P. 2011. Spatio-Temporal Heterogeneity: Concepts and Analyses. Cambridge University Press

Fang X Q, Chen F H. 2015. Plant phenology and climate change. Sci China Earth Sci, 58: 1043–1044

Ge Q S, Dai J H, Cui H J, Wang H J. 2016. Spatiotemporal variability in start and end of growing season in China related to climate variability. Remote Sens, 8: 433

Ge Q S, Wang H J, Zheng J Y, Rutishauser T, Dai J H. 2014. A 170 year spring phenology index of plants in eastern China. J Geophys Res-Biogeosci, 119: 301–311

Ge Q S, Wang H J, Rutishauser T, Dai J H. 2015. Phenological response to climate change in China: A meta-analysis. Glob Change Biol, 21: 265–274

Gordo O, Sanz J J. 2010. Impact of climate change on plant phenology in Mediterranean ecosystems. Glob Change Biol, 16: 1082–1106

Guo Q H, Hu T Y, Jiang Y Q, Jin S C, Wang R, Guan H C, Yang Q L, Li Y M, Wu F F, Zhai Q P, Liu J, Su Y J. 2018. Advances in remote sensing application for biodiversity research (in Chinese). Biodivers Sci, 26: 9–26

Han J W, Kamber M, Pei J. 2012. Data Mining Concepts and Techniques. Waltham: Morgan Kaufman MIT Press

Hoffman F M, Kumar J, Mills R T, Hargrove W W. 2013. Representativeness-based sampling network design for the State of Alaska. Landscape Ecol, 28: 1567–1586

Izquierdo-Verdiguier E, Zurita-Milla R, Ault T R, Schwartz M D. 2018. Development and analysis of spring plant phenology products: 36 years of 1-km grids over the conterminous US. Agric For Meteorol, 262: 34–41

Jeong S J, Ho C H, Gim H J, Brown M E. 2011. Phenology shifts at start vs. end of growing season in temperate vegetation over the Northern Hemisphere for the period 1982–2008. Glob Change Biol, 17: 2385–2399

Kelling S, Hochachka W M, Fink D, Riedewald M, Caruana R, Ballard G, Hooker G. 2009. Data-intensive science: A new paradigm for biodiversity studies. BioScience, 59: 613–620

Kisilevich S, Mansmann F, Nanni M, Rinzivillo S. 2010. Spatio-temporal clustering. In: Maimon O, Rokach L, eds. Data Mining and Knowledge Discovery Handbook. Boston: Springer. 855–874

Kumar J, Mills R T, Hoffman F M, Hargrove W W. 2011. Parallel *k*-means clustering for quantitative ecoregion delineation using large data sets. Procedia Comput Sci, 4: 1602–1611

La Salle J, Williams K J, Moritz C. 2016. Biodiversity analysis in the digital era. Phil Trans R Soc B, 371: 20150337

Li X, Zhao N, Jin R, Liu S M, Sun X M, Wen X F, Wu D X, Zhou Y, Guo J W, Chen S P. 2019. Internet of Things to network smart devices for ecosystem monitoring. Chin Sci Bull, 64: 1234–1245

Lu P L. 2006. Responses of Chinese woody plants phenology to climatic change (in Chinese). Dissertation for Doctoral Degree. Beijing Forestry University

Piao S L, Fang J Y, Zhou L M, Ciais P, Zhu B. 2006. Variations in satellite-

derived phenology in China's temperate vegetation. Glob Change Biol, 12: 672–685
Piao S L, Tan J G, Chen A P, Fu Y S, Ciais P, Liu Q, Janssens I A, Vicca S, Zeng Z Z, Jeong S J. 2015. Leaf onset in the northern hemisphere triggered by daytime temperature. Nat Commun, 6: 6911
Peng S S, Chen A P, Xu L, Cao C X, Fang J Y, Myneni R B, Pinzon J E, Tucker C J, Piao S L. 2011. Recent change of vegetation growth trend in China. Environ Res Lett, 6: 27–44
Rousseeuw P J. 1987. Silhouettes: A graphical aid to the interpretation and validation of cluster analysis. J Comput Appl Math, 20: 53–65
Ruml M, Vulić T. 2005. Importance of phenological observations and predictions in agriculture. J Agric Sci BGD, 50: 217–225
Schwartz M D, Ahas R, Aasa A. 2006. Onset of spring starting earlier across the Northern Hemisphere. Glob Change Biol, 12: 343–351
Schwartz M D, Ault T R, Betancourt J L. 2013. Spring onset variations and trends in the continental United States: Past and regional assessment using temperature-based indices. Int J Climatol, 33: 2917–2922
Schwartz M D, Chen X Q. 2002. Examining the onset of spring in China. Clim Res, 21: 157–164
Shen S, Cheng C X, Song C Q, Yang J, Yang S L, Su K, Yuan L H, Chen X Q. 2018. Spatial distribution patterns of global natural disasters based on biclustering. Nat Hazards, 92: 1809–1820
Wan M W, Liu X Z. 1979. The Methodology of Phenological Observations in China (in Chinese). Beijing: Science Press
Wang H J, Dai J H, Zheng J Y, Ge Q S. 2015a. Temperature sensitivity of plant phenology in temperate and subtropical regions of China from 1850 to 2009. Int J Climatol, 35: 913–922
Wang H J, Ge Q S, Dai Y X, Dai J H. 2015b. Parameterization of temperature sensitivity of spring phenology and its application in explaining diverse phenological responses to temperature change. Sci Rep, 5: 8833
Wang J F, Zhang T L, Fu B J. 2016. A measure of spatial stratified heterogeneity. Ecol Indic, 67: 250–256
Wang J F, Xu C D. 2017. Geodetector: Principle and prospective (in Chinese). Acta Geogr Sin, 72: 116–134
Wang X F, Xiao J F, Li X, Cheng G D, Ma M G, Zhu G F, Arain M A, Black T A, Jassal R S. 2019. No trends in spring and autumn phenology during the global warming hiatus. Nat Commun, 10: 2389
White M A, de BEURS K M, Didan K, Inouye D W, Richardson A D, Jensen O P, O'keefe J, Zhang G, Nemani R R, van LEEUWEN W J D, Brown J F, de WIT A, Schaepman M, Lin X, Dettinger M, Bailey A S, Kimball J, Schwartz M D, Baldocchi D D, Lee J T, Lauenroth W K. 2009. Intercomparison, interpretation, and assessment of spring phenology in North America estimated from remote sensing for 1982–2006. Glob Change Biol, 15: 2335–2359
White M A, Hoffman F, Hargrove W W, Nemani R R. 2005. A global framework for monitoring phenological responses to climate change. Geophys Res Lett, 32: L04705
Wu X C, Liu H Y. 2013. Consistent shifts in spring vegetation green-up date across temperate biomes in China, 1982–2006. Glob Change Biol, 19: 870–880
Wu X J, Zurita-Milla R, Kraak M J. 2015. Co-clustering geo-referenced time series: Exploring spatio-temporal patterns in Dutch temperature data. Int J Geogr Inf Sci, 29: 624–642
Wu X J, Zurita-Milla R, Kraak M J. 2016. A novel analysis of spring phenological patterns over Europe based on co-clustering. J Geophys Res-Biogeosci, 121: 1434–1448
Zhang Y, Hepner G F, Dennison P E. 2012. Delineation of phenoregions in geographically diverse regions using *k*-means++ clustering: A case study in the Upper Colorado River Basin. GISci Remote Sens, 49: 163–181
Zhu D, Wang N H, Wu L, Liu Y. 2017. Street as a big geo-data assembly and analysis unit in urban studies: A case study using Beijing taxi data. Appl Geogr, 86: 152–164
Zhu K Z, Wan M W. 1973. Phenology (in Chinese). Beijing: Science Press
Zirlewagen D, von Wilpert K. 2010. Upscaling of environmental information: Support of land-use management decisions by spatio-temporal regionalization approaches. Environ Manage, 46: 878–893

(Responsible editor: Xin LI)